International Journal of Thermal Sciences 49 (2010) 571–579

Contents lists available at ScienceDirect

International Journal of Thermal Sciences

journal homepage: www.elsevier.com/locate/ijts

A new accurate finite difference scheme for Neumann (insulated) boundary condition of heat conduction

Weizhong Dai*

Mathematics and Statistics, College of Engineering and Science, Louisiana Tech University, Ruston, LA 71272, USA

ARTICLE INFO

Article history:
Received 19 June 2009
Received in revised form
26 August 2009
Accepted 27 August 2009
Available online 16 September 2009

Keywords:
Neumann (insulated) boundary condition
Heat conduction
Crank–Nicholson scheme
Higher-order scheme
Stability

ABSTRACT

The Neumann (or insulated) boundary condition is often encountered in engineering applications. The conventional finite difference schemes are either first-order accurate or second-order accurate but need a ghost point outside the boundary. Compact finite difference schemes are difficult to apply for multi-dimensional cases or for cylindrical and spherical coordinate cases. In this study, we present a kind of new and accurate finite difference schemes for the Neumann (insulated) boundary condition in Cartesian, cylindrical, and spherical coordinates, respectively. Combined with the Crank–Nicholson finite difference method or other higher-order methods, the overall scheme is proved to be unconditionally stable and provides much more accurate numerical solutions. The numerical errors and convergence rates of the solution are tested by several examples. Results show that the new method is promising.

1. Introduction

The Neumann (or insulated) boundary condition is often encountered in engineering applications, such as ultrafast heat transfer [1–7] and reaction-diffusions [8–12]. The conventional finite difference schemes for the Neumann boundary condition are either first-order accurate or second-order accurate but need a ghost point outside the boundary [13–15]. We have found that, when the first-order accurate scheme for the Neumann boundary condition is employed, it affects the accuracy of the overall numerical solution even if a second-order numerical scheme is employed at interior grid points. Also, when the second-order accurate finite difference scheme (or the ghost point method [15]) for the Neumann boundary condition is employed, the overall scheme may not be unconditionally stable (that is, there are some restrictions on the mesh ratio). Furthermore, the ghost point method may be difficult to apply for the multi-dimensional disk or sphere in cylindrical or spherical coordinates. Recently, Liao et al. [12] have proposed a third-order compact finite difference scheme for the Neumann boundary condition. However, the scheme becomes complicated when applied to multi-dimensional cases or to cylindrical and spherical coordinate cases. Zhao and Dai [16,17] have also developed a second-order combined compact finite difference scheme for the Neumann boundary condition. When applying it to cylindrical and spherical coordinate cases, we found that it reduces the order of accuracy in numerical solutions. In this study, we consider one-dimensional heat conduction problems with the Neumann (or insulated) boundary condition in Cartesian, cylindrical, and spherical coordinates, respectively, and present a kind of new and accurate finite difference schemes for the Neumann boundary condition. Combined with the Crank–Nicholson finite difference method or the higher-order compact finite difference method, the overall scheme provides much more accurate numerical solutions. Furthermore, the overall scheme can be proved to be unconditionally stable. The numerical errors and convergence rates of the solutions are then tested by several examples.

2. Finite difference schemes

In this section, we consider the Neumann boundary condition in Cartesian, cylindrical, and spherical coordinates, respectively, and develop the corresponding finite difference schemes.

CASE 1. We first consider a one-dimensional heat conduction equation with initial and Neumann boundary conditions in Cartesian coordinates:

$$C\frac{\partial T(x,t)}{\partial t} = k\frac{\partial^2 T(x,t)}{\partial x^2} + s(x,t), \quad 0 < x < L, 0 < t \le t_0, \tag{1a}$$

$$T(x,0) = T_0(x), \quad x \in [0,L], \tag{1b}$$

* Tel.: +1 318 257 3301; fax: +1 318 257 2562.
E-mail address: dai@coes.latech.edu

1290-0729/$ – see front matter © 2009 Elsevier Masson SAS. All rights reserved.
doi:10.1016/j.ijthermalsci.2009.08.007

Nomenclature

a, a^*, b, b^*, c, c^*	constants
C	volumetric heat capacity [J/(m^{3}K)]
E	l_2-norm error
h	spatial grid size
k	conductivity [W/(mK)]
L	length [m]
M	number of grid points
P_r	finite difference operator
r	radius coordinate
$r_j, r_{j+\frac{1}{2}}$	grid point along the r-direction
s	source term [J/(m^{3}s)]
T	temperature [K]
T_j^n	numerical solution of T at $(jh, n\Delta t)$
t, t_0	time [s]
x	Cartesian coordinate
x_j	grid point along the x-direction

Greek symbols

$\nabla_{\bar{r}}$	backward finite difference operator
Δt	time increment
θ_1, θ_2	constants

Subscript, superscript

j	the jth grid point
n	the nth time level

$$\frac{\partial T(0,t)}{\partial x} = \frac{\partial T(L,t)}{\partial x} = 0, \quad t\in[0,t_0], \tag{1c}$$

where $T(x, t)$ is temperature, C is heat capacity, k is conductivity, and $s(x, t)$ is a source term. To solve the above problem using the finite difference method, one may employ the Crank–Nicholson scheme for Eq. (1a) as follows:

$$C\frac{T_j^{n+1}-T_j^n}{\Delta t} = k\frac{T_{j-1}^{n+1}-2T_j^{n+1}+T_{j+1}^{n+1}}{2h^2} + k\frac{T_{j-1}^{n}-2T_j^{n}+T_{j+1}^{n}}{2h^2} + s_j^{n+\frac{1}{2}}, \quad 1\le j\le M-1, \tag{2}$$

where T_j^n is the numerical approximation of $T(jh, n\Delta t)$. Here, h and Δt are the spatial and temporal mesh sizes, respectively, and $x_j = jh$, $0 \le j \le M$ such that $Mh = L$. On the other hand, the boundary condition, Eq. (1c), can be discretized by using the conventional finite difference method [13–15] such as the first-order accurate scheme

$$T_0^n = T_1^n, \quad T_M^n = T_{M-1}^n, \tag{3}$$

or the second-order accurate scheme

$$T_{-1}^n = T_1^n, \quad T_{M+1}^n = T_{M-1}^n, \tag{4}$$

where T_{-1}^n and T_{M+1}^n are the fictitious temperatures outside the boundary. It should be pointed out that in order to employ Eq. (4), one must couple it with Eq. (2) by letting $j = 0$ and M, so that T_{-1}^{n+1} and T_{M+1}^{n+1} can be eliminated.

To obtain a new finite difference scheme for the Neumann boundary condition, Eq. (1c), we first design a mesh, where the distance between the actual left boundary and x_1 is assumed to be $\theta_1 h$, and the distance between the actual right boundary and x_M is $\theta_2 h$, as shown in Fig. 1. We then express the finite difference approximation of $\partial^2 T(x,t)/\partial x^2$ at x_1, which is the point next to the left boundary, as follows:

$$b\frac{\partial^2 T(x_1,t)}{\partial x^2} = \frac{a}{h^2}[T(x_2,t)-T(x_1,t)] - \frac{1}{h}\frac{\partial T(x_1-\theta_1 h,t)}{\partial x}, \tag{5}$$

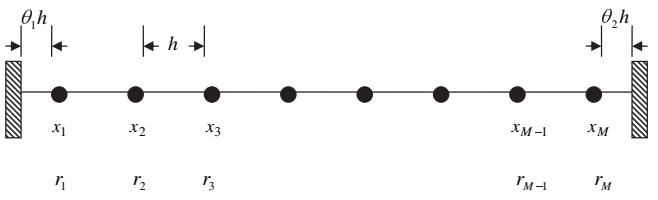

Fig. 1. Mesh and locations of grid points.

where a, b, θ_1 are constants to be determined. If Eq. (5) is rewritten as follows:

$$b\frac{\partial^2 T(x_1,t)}{\partial x^2} + \frac{1}{h}\frac{\partial T(x_1-\theta_1 h,t)}{\partial x} = \frac{a}{h^2}[T(x_2,t)-T(x_1,t)], \tag{5'}$$

one may see that the above equation is an improvement of the combined compact finite difference method (where the first and second-order derivatives are included [16–18]) by introducing the parameter θ_1 in order to raise the order of accuracy. The first-order derivative is kept in Eq. (5) so that the Neumann boundary condition can be applied directly without discretizing. Expanding each term of Eq. (5) into Taylor series at x_1, we obtain the right-hand-side (RHS) result of Eq. (5) as follows:

$$\begin{aligned}\text{RHS} &= \frac{a}{h^2}\left[hT_x(x_1,t)+\frac{h^2}{2}T_{xx}(x_1,t)+\frac{h^3}{6}T_{x^3}(x_1,t)\right] \\ &\quad -\frac{1}{h}\left[T_x(x_1,t)-\theta_1 hT_{xx}(x_1,t)+\frac{\theta_1^2h^2}{2}T_{x^3}(x_1,t)\right]+O(h^2) \\ &= \frac{1}{h}[a-1]T_x(x_1,t)+\left[\frac{a}{2}+\theta_1\right]T_{xx}(x_1,t)+\frac{h}{2}\left[\frac{a}{3}-\theta_1^2\right]T_{x^3}(x_1,t) \\ &\quad +O(h^2).\end{aligned} \tag{6}$$

Matching both sides gives

$$a = 1, \quad b = \frac{1}{2}+\frac{\sqrt{3}}{3}, \quad \theta_1 = \frac{\sqrt{3}}{3}. \tag{7}$$

Thus, substituting the values of a, b, θ_1 in Eq. (7) into Eq. (5) and dropping the truncation error $O(h^2)$, we obtain a second-order finite difference approximation at x_1 as

$$\frac{\partial^2 T(x_1,t)}{\partial x^2} \approx \frac{a}{bh^2}[T(x_2,t)-T(x_1,t)] - \frac{1}{bh}\frac{\partial T(x_1-\theta_1 h,t)}{\partial x}. \tag{8}$$

Symmetrically, we can express the finite difference approximation of $\partial^2 T(x,t)/\partial x^2$ at x_M, which is the point next to the right boundary, as

$$b^*\frac{\partial^2 T(x_M,t)}{\partial x^2} = \frac{1}{h}\frac{\partial T(x_M+\theta_2 h,t)}{\partial x} - \frac{a^*}{h^2}[T(x_M,t)-T(x_{M-1},t)], \tag{9}$$

where a^*, b^*, θ_2 are constants to be determined. Again, matching both sides in Taylor series gives

$$a^* = 1, \quad b^* = \frac{1}{2}+\frac{\sqrt{3}}{3}, \quad \theta_2 = \frac{\sqrt{3}}{3}, \tag{10}$$

and hence a second-order finite difference approximation at x_M for the right boundary can be obtained as

$$\frac{\partial^2 T(x_M,t)}{\partial x^2} \approx \frac{1}{b^* h}\frac{\partial T(x_M+\theta_2 h,t)}{\partial x} - \frac{a^*}{b^* h^2}[T(x_M,t)-T(x_{M-1},t)]. \quad (11)$$

If the number of interior grid points M is given, then the grid size and the coordinates of the grid points can be determined as follows:

$$h = \frac{L}{M+\theta_1+\theta_2-1}, \quad x_j = (j-1+\theta_1)h, \quad j = 1,\cdots,M. \quad (12)$$

Using the Neumann boundary condition, Eq. (1c), one may simplify Eqs. (9) and (11) to

$$\frac{\partial^2 T(x_1,t)}{\partial x^2} \approx \frac{a}{bh^2}[T(x_2,t) - T(x_1,t)], \quad (13a)$$

$$\frac{\partial^2 T(x_M,t)}{\partial x^2} \approx -\frac{a^*}{b^* h^2}[T(x_M,t) - T(x_{M-1},t)]. \quad (13b)$$

It should be pointed out that the Neumann boundary condition is directly used in Eq. (13) without discretizing. Thus, the Crank–Nicholson scheme for Eq. (1a) at x_1 and x_M can be written as follows:

$$C\frac{T_1^{n+1}-T_1^n}{\Delta t} = k\frac{a}{b}\frac{T_2^{n+1}-T_1^{n+1}}{2h^2} + k\frac{a}{b}\frac{T_2^n - T_1^n}{2h^2} + s_1^{n+\frac{1}{2}}, \quad (14a)$$

$$C\frac{T_M^{n+1}-T_M^n}{\Delta t} = -k\frac{a^*}{b^*}\frac{T_M^{n+1}-T_{M-1}^{n+1}}{2h^2} - k\frac{a^*}{b^*}\frac{T_M^n - T_{M-1}^n}{2h^2} + s_M^{n+\frac{1}{2}}. \quad (14b)$$

Hence, a new second-order accurate Crank–Nicholson finite difference scheme consists of Eq. (2) for interior grid points x_j where $j = 2, \ldots, M-1$, and Eq. (14) for two grid points x_1 and x_M. It can be seen that the truncation error of the new scheme has an order of $\Delta t^2 + h^2$ at all grid points $(x_j, t_{n+(1/2)}), j = 1,\cdots,M$.

CASE 2. We now consider a one-dimensional heat conduction equation with initial and Neumann boundary conditions in cylindrical coordinates:

$$C\frac{\partial T(r,t)}{\partial t} = \frac{k}{r}\frac{\partial}{\partial r}\left(r\frac{\partial T(r,t)}{\partial r}\right) + s(r,t), \; 0<r<L, 0<t\le t_0, \quad (15a)$$

$$T(r,0) = T_0(r), \quad r\in[0,L], \quad (15b)$$

$$\frac{\partial T(0,t)}{\partial r} = \frac{\partial T(L,t)}{\partial r} = 0, \quad t\in[0,t_0]. \quad (15c)$$

To obtain a second-order accurate finite difference scheme for the Neumann boundary condition, we similarly design a mesh, where the distance between the actual left boundary and r_1 is assumed to be $\theta_1 h$, and the distance between the actual right boundary and r_M is $\theta_2 h$, as shown in Fig. 1. We then express the finite difference approximation of $(\partial/\partial r)(r(\partial T(r,t)/\partial r))$ at r_1, which is the point next to the left boundary, as follows:

$$b\frac{\partial}{\partial r}\left(r\frac{\partial T(r,t)}{\partial r}\right)_1 = \frac{a}{h^2}r_{\frac{3}{2}}[T(r_2,t)-T(r_1,t)] - \frac{1}{h}r_1\frac{\partial T(r_1-\theta_1 h,t)}{\partial r}, \quad (16)$$

where a, b, θ_1 are constants to be determined and $r_{3/2} = r_1 + (h/2)$. If each term of Eq. (16) is expanded into Taylor series at r_1, we will obtain the left-hand-side (LHS) and right-hand-side (RHS) results of Eq. (16) as follows:

$$\text{LHS} = bT_r(r_1,t) + br_1 T_{rr}(r_1,t) \quad (17a)$$

and

$$\begin{aligned}\text{RHS} &= \frac{a}{h^2}r_{\frac{3}{2}}\left[hT_r(r_1,t) + \frac{h^2}{2}T_{rr}(r_1,t) + \frac{h^3}{6}T_{r^3}(r_1,t)\right] \\ &\quad - \frac{1}{h}r_1\left[T_r(r_1,t) - \theta_1 hT_{rr}(r_1,t) + \frac{\theta_1^2 h^2}{2}T_{r^3}(r_1,t)\right] + O(h^2) \\ &= \frac{1}{h}\left[ar_{\frac{3}{2}} - r_1\right]T_r(r_1,t) + \left[\frac{a}{2}r_{\frac{3}{2}} + r_1\theta_1\right]T_{rr}(r_1,t) \\ &\quad + \frac{h}{2}\left[\frac{a}{3}r_{\frac{3}{2}} - r_1\theta_1^2\right]T_{r^3}(r_1,t) + O(h^2). \end{aligned} \quad (17b)$$

Matching both sides gives

$$\frac{1}{h}(ar_{\frac{3}{2}} - r_1) = b, \quad (18a)$$

$$\frac{a}{2}r_{\frac{3}{2}} + r_1\theta_1 = br_1, \quad (18b)$$

$$\frac{a}{3}r_{\frac{3}{2}} - r_1\theta_1^2 = 0. \quad (18c)$$

Dividing Eq. (18a) by Eq. (18b), replacing $ar_{3/2}$ with $3r_1\theta_1^2$ from Eq. (18c) and then using the fact $r_1 = \theta_1 h$, we obtain a quadratic equation with respect to θ_1 as

$$6\theta_1^2 - 3\theta_1 - 4 = 0. \quad (19)$$

Solving the above equation for θ_1 with $\theta_1 \ge 0$, one may obtain

$$\theta_1 = \frac{3+\sqrt{105}}{12}, \quad \frac{a}{b} = \frac{r_1\theta_1}{r_{\frac{3}{2}}\left(\frac{\theta_1}{2}+\frac{1}{3}\right)}. \quad (20)$$

Thus, a second-order finite difference approximation at r_1 can be obtained by dropping the truncation error $O(h^2)$:

$$\frac{\partial}{\partial r}\left(r\frac{\partial T(r,t)}{\partial r}\right)_1 \approx \frac{a}{bh^2}r_{\frac{3}{2}}[T(r_2,t)-T(r_1,t)] - \frac{1}{bh}r_1\frac{\partial T(r_1-\theta_1 h,t)}{\partial r}. \quad (21)$$

We have noted that $\theta_1 > 1$ in Eq. (20) while $\theta_1 < 1$ in Eq. (7). This is probably because, in the cylindrical coordinates, the term $(\partial/\partial r)(r(\partial T(r,t)/\partial r)) = rTrr(r,\ t) + Tr(r,t)$ includes the first-order derivative of $T(r,t)$.

Symmetrically, we express the finite difference approximation of $(\partial/\partial r)(r(\partial T(r,t)/\partial r))$ at r_M, which is the point next to the right boundary, as

$$\begin{aligned} b^*\frac{\partial}{\partial r}\left(r\frac{\partial T(r,t)}{\partial r}\right)_M &= \frac{1}{h}r_M\frac{\partial T(r_M+\theta_2 h,t)}{\partial r} - \frac{a^*}{h^2}r_{M-\frac{1}{2}}[T(r_M,t) \\ &\quad - T(r_{M-1},t)], \end{aligned} \quad (22)$$

where a^*, b^*, θ_2 are constants to be determined and $r_{M-(1/2)} = r_M - (h/2)$. Again, matching both sides in Taylor series gives

$$\frac{1}{h}\left(r_M - a^* r_{M-\frac{1}{2}}\right) = b^*, \quad (23a)$$

$$r_M\theta_2 + \frac{a^*}{2}r_{M-\frac{1}{2}} = b^* r_M, \quad (23b)$$

$$r_M\theta_2^2 - \frac{a^*}{3}r_{M-\frac{1}{2}} = 0. \quad (23c)$$

Dividing Eq. (23a) by Eq. (23b) and then replacing $a^* r_{M-(1/2)}$ by $3r_M\theta_2^2$ from Eq. (23c), we obtain a quadratic equation with respect to θ_2 as

$$(6r_M + 3h)\theta_2^2 + 2h\theta_2 - 2r_M = 0. \tag{24}$$

If the number of interior grid points M is given, then the grid size and the coordinates of the grid points can be determined as follows:

$$h = \frac{L}{M+\theta_1+\theta_2-1}, \quad r_j = (j-1+\theta_1)h, \quad j = 1,\cdots,M. \tag{25}$$

Substituting Eq. (25) into Eq. (24) and then solving for θ_2 with $\theta_2 \geq 0$, one may obtain

$$\theta_2 = \frac{\sqrt{1+6(2\theta_1+2M-1)(\theta_1+M-1)}-1}{3(2\theta_1+2M-1)}, \text{ and}$$
$$\frac{a^*}{b^*} = \frac{r_M\theta_2}{r_{M-\frac{1}{2}}\left(\frac{\theta_2}{2}+\frac{1}{3}\right)}, \tag{26}$$

and, hence, a second-order finite difference approximation at r_M can be obtained:

$$\frac{\partial}{\partial r}\left(r\frac{\partial T(r,t)}{\partial r}\right)_M \approx \frac{1}{b^*h}r_M\frac{\partial T(r_M+\theta_2 h,t)}{\partial r} - \frac{a^*}{b^*h^2}r_{M-\frac{1}{2}}[T(r_M,t) - T(r_{M-1},t)]. \tag{27}$$

Using the Neumann boundary condition, Eq. (15c), one may simplify Eqs. (21) and (27) to

$$\frac{\partial}{\partial r}\left(r\frac{\partial T(r,t)}{\partial r}\right)_1 \approx \frac{a}{bh^2}r_{\frac{3}{2}}[T(r_2,t)-T(r_1,t)], \tag{28a}$$

$$\frac{\partial}{\partial r}\left(r\frac{\partial T(r,t)}{\partial r}\right)_M \approx -\frac{a^*}{b^*h}r_{M-\frac{1}{2}}[T(r_M,t)-T(r_{M-1},t)]. \tag{28b}$$

Thus, the Crank–Nicholson scheme for Eq. (15a) can be written as follows:

$$C\frac{T_1^{n+1}-T_1^n}{\Delta t} = k\frac{a}{br_1}r_{\frac{3}{2}}\frac{T_2^{n+1}-T_1^{n+1}}{2h^2} + k\frac{a}{br_1}r_{\frac{3}{2}}\frac{T_2^n-T_1^n}{2h^2} + s_1^{n+\frac{1}{2}}, \tag{29a}$$

$$C\frac{T_j^{n+1}-T_j^n}{\Delta t} = k\frac{1}{2h^2r_j}\left[r_{j+\frac{1}{2}}\left(T_{j+1}^{n+1}-T_j^{n+1}\right) - r_{j-\frac{1}{2}}\left(T_j^{n+1}-T_{j-1}^{n+1}\right)\right] + k\frac{1}{2h^2r_j}\left[r_{j+\frac{1}{2}}\left(T_{j+1}^{n}-T_j^{n}\right) - r_{j-\frac{1}{2}}\left(T_j^{n}-T_{j-1}^{n}\right)\right] + s_j^{n+\frac{1}{2}}, \quad 2 \leq j \leq M-1, \tag{29b}$$

$$C\frac{T_M^{n+1}-T_M^n}{\Delta t} = -k\frac{a^*}{b^*r_j}r_{M-\frac{1}{2}}\frac{T_M^{n+1}-T_{M-1}^{n+1}}{2h^2} - k\frac{a^*}{b^*r_j}r_{M-\frac{1}{2}}\frac{T_M^n-T_{M-1}^n}{2h^2} + s_M^{n+\frac{1}{2}}. \tag{29c}$$

Again, it can be seen that the truncation error of the new scheme has an order of $\Delta t^2 + h^2$ at all grid points $(r_j, t_{n+(1/2)}) j = 1,\cdots,M$.

It should be pointed out that, in the ghost point method [13–15], the term $(1/r)(\partial/\partial r)(r(\partial T(r,t)/\partial r))$ in Eq. (15a) is first evaluated based on the boundary condition, Eq. (15c), to obtain $\lim_{r\to 0}[(1/r)(\partial/\partial r)(r(\partial T(r,t)/\partial r))] = \lim_{r\to 0}\left[\frac{\partial^2 T(r,t)}{\partial r^2} + \frac{1}{r}\frac{\partial T(r,t)}{\partial r}\right] = 2\frac{\partial^2 T(0,t)}{\partial r^2}$ at the boundary point $r = 0$, and then the term $2(\partial^2 T(0,t)/\partial r^2)$ is discretized to be $(1/h^2)[(T_1^{n+1} - 2T_0^{n+1} + T_{-1}^{n+1}) + (T_1^n - 2T_0^n + T_{-1}^n)]$, where $T_{-1}{}^{n+1} = T_1{}^{n+1}$ and $T_{-1}{}^n = T_1{}^n$. However, the ghost point scheme cannot be generalized to multi-dimensional heat conduction cases such as $(\partial T(r,\phi,t)/\partial t) = (C/r)(\partial/\partial r)(r(\partial T(r,\phi,t)/\partial r)) + (C/r^2)(\partial^2 T(r,\phi,t)/\partial\phi^2)$, because $\lim_{r\to 0}[(1/r^2)(\partial^2 T(r,\phi,t)/\partial\phi^2)]$ is difficult to find. On the other hand, our present scheme can be easily generalized to the multi-dimensional heat conduction equation because we avoid the approximation at $r = 0$.

CASE 3. We consider a one-dimensional heat conduction equation with initial and Neumann boundary conditions in spherical coordinates:

$$C\frac{\partial T(r,t)}{\partial t} = \frac{k}{r^2}\frac{\partial}{\partial r}\left(r^2\frac{\partial T(r,t)}{\partial r}\right) + s(r,t), \; 0<r<L, 0<t\leq t_0, \tag{30a}$$

$$T(r,0) = T_0(r), \quad r\in[0,L], \tag{30b}$$

$$\frac{\partial T(0,t)}{\partial r} = \frac{\partial T(L,t)}{\partial r} = 0, \quad t\in[0,t_0]. \tag{30c}$$

Similarly, we use a mesh as shown in Fig. 1 and express the finite difference approximation of $(\partial/\partial r)(r^2(\partial T(r,t)/\partial r))$ at r_1 as follows:

$$b\frac{\partial}{\partial r}\left(r^2\frac{\partial T(r,t)}{\partial r}\right)_1 = \frac{a}{h^2}r_{\frac{3}{2}}^2[T(r_2,t)-T(r_1,t)] - \frac{1}{h}r_1^2\frac{\partial T(r_1-\theta_1\Delta r,t)}{\partial r}, \tag{31}$$

where a, b, θ_1 are constants to be determined and $r_{3/2} = r_1 + (h/2)$. Again, if each term of Eq. (31) is expanded into Taylor series at r_1, we will obtain the left-hand-side (LHS) and right-hand-side (RHS) results of Eq. (31) as follows:

$$\text{LHS} = 2br_1T_r(r_1,t) + br_1^2T_{rr}(r_1,t), \tag{32a}$$

$$\begin{aligned}\text{RHS} &= \frac{a}{h^2}r_{\frac{3}{2}}^2\left[hT_r(r_1,t) + \frac{h^2}{2}T_{rr}(r_1,t) + \frac{h^3}{6}T_{r^3}(r_1,t)\right] \\ &\quad - \frac{1}{h}r_1^2\left[T_r(r_1,t) - \theta_1 hT_{rr}(r_1,t) + \frac{\theta_1^2h^2}{2}T_{r^3}(r_1,t)\right] + O(h^2) \\ &= \frac{1}{h}\left[ar_{\frac{3}{2}}^2 - r_1^2\right]T_r(r_1,t) + \left[\frac{a}{2}r_{\frac{3}{2}}^2 + r_1^2\theta_1\right]T_{rr}(r_1,t) \\ &\quad + \frac{h}{2}\left[\frac{a}{3}r_{\frac{3}{2}}^2 - r_1^2\theta_1^2\right]T_{r^3}(r_1,t) + O(h^2).\end{aligned} \tag{32b}$$

Matching both sides gives

$$\frac{1}{h}\left(ar_{\frac{3}{2}}^2 - r_1^2\right) = 2br_1, \tag{33a}$$

$$\frac{a}{2}r_{\frac{3}{2}}^2 + r_1^2\theta_1 = br_1^2, \tag{33b}$$

$$\frac{a}{3}r_{\frac{3}{2}}^2 - r_1^2\theta_1^2 = 0. \tag{33c}$$

Dividing Eq. (33a) by Eq. (33b) and then replacing $ar_{3/2}^2$ with $3r_1^2\theta_1^2$ from Eq. (33c), we obtain a quadratic equation with respect to θ_1 as

$$\theta_1^2 - \theta_1 - 1 = 0 \tag{34}$$

Solving the above equation for θ_1 with $\theta_1 \geq 0$, one may obtain

$$\theta_1 = \frac{\sqrt{5}+1}{2}, \quad \frac{a}{b} = \frac{r_1^2\theta_1}{r_{\frac{3}{2}}^2\left(\frac{\theta_1}{2}+\frac{1}{3}\right)}. \tag{35}$$

It can be seen that $\theta_1 > 1$ in Eq. (35), which is similar to the one in Eq. (21). Thus, a second-order finite difference approximation at r_1 can be obtained by dropping the truncation error $O(h^2)$:

$$\frac{\partial}{\partial r}\left(r^2\frac{\partial T(r,t)}{\partial r}\right)_1 \approx \frac{a}{bh^2}\, r_{\frac{3}{2}}^2\left[T(r_2,t)-T_j(r_1,t)\right] - \frac{1}{bh}\, r_1^2\frac{\partial T(r_1-\theta_1 h,t_n)}{\partial r}. \tag{36}$$

Symmetrically, we express the finite difference approximation of $(\partial/\partial r)(r^2(\partial T(r,t)/\partial r))$ at r_M, which is the point next to the right boundary, as

$$b^*\frac{\partial}{\partial r}\left(r^2\frac{\partial T(r,t)}{\partial r}\right)_M = \frac{1}{h}r_M^2\frac{\partial T(r_M+\theta_2 h,t)}{\partial r} - \frac{a^*}{h^2}r_{M-\frac{1}{2}}^2[T(r_M,t)-T(r_{M-1},t)], \tag{37}$$

where a^*, b^*, θ_2 are constants to be determined and $r_{M-(1/2)} = r_M - (h/2)$. Again, matching both sides in Taylor series gives

$$\frac{1}{h}\left(r_M^2 - a^* r_{M-\frac{1}{2}}^2\right) = 2b^* r_M, \tag{38a}$$

$$r_M^2\theta_2 + \frac{a^*}{2}\, r_{M-\frac{1}{2}}^2 = b^* r_M^2, \tag{38b}$$

$$r_M^2\theta_2^2 - \frac{a^*}{3}\, r_{M-\frac{1}{2}}^2 = 0. \tag{38c}$$

Dividing Eq. (38a) by Eq. (38b) and then replacing $a^* r_{M-(1/2)}^2$ with $3r_M^2\theta_2^2$ from Eq. (38c), we obtain a quadratic equation with respect to θ_2 as

$$(3r_M + 3h)\theta_2^2 + 2h\theta_2 - r_M = 0. \tag{39}$$

If the number of interior grid points M is given, then the grid size and the coordinates of the grid points can be determined as follows:

$$h = \frac{L}{M+\theta_1+\theta_2-1}, \quad r_j = (j-1+\theta_1)h, \quad j = 1,\cdots,M. \tag{40}$$

Thus, we obtain

$$\theta_2 = \frac{\sqrt{4+3(\theta_1+M)(\theta_1+M-1)}-1}{3(\theta_1+M)}, \text{ and } \frac{a^*}{b^*} = \frac{r_M^2\theta_2}{r_{M-\frac{1}{2}}^2\left(\frac{\theta_2}{2}+\frac{1}{3}\right)}. \tag{41}$$

Hence, the Crank–Nicholson scheme for Eq. (30a) coupled with Eq. (30c) can be written as follows:

$$C\frac{T_1^{n+1}-T_1^n}{\Delta t} = k\frac{a}{br_1^2}\; r_{\frac{3}{2}}^2\frac{T_2^{n+1}-T_1^{n+1}}{2h^2} + k\frac{a}{br_1^2}\; r_{\frac{3}{2}}^2\frac{T_2^n-T_1^n}{2h^2} + s_1^{n+\frac{1}{2}}, \tag{42a}$$

$$C\frac{T_j^{n+1}-T_j^n}{\Delta t} = k\frac{1}{2h^2r_j^2}\left[r_{j+\frac{1}{2}}^2\left(T_{j+1}^{n+1}-T_j^{n+1}\right) - r_{j-\frac{1}{2}}^2\left(T_j^{n+1}-T_{j-1}^{n+1}\right)\right] + k\frac{1}{2h^2r_j^2}\left[r_{j+\frac{1}{2}}^2\left(T_{j+1}^{n}-T_j^{n}\right) - r_{j-\frac{1}{2}}^2\left(T_j^{n}-T_{j-1}^{n}\right)\right] + s_j^{n+\frac{1}{2}}, \quad 2\le j\le M-1, \tag{42b}$$

$$C\frac{T_M^{n+1}-T_M^n}{\Delta t} = -k\frac{a^*}{b^*r_M^2}r_{M-\frac{1}{2}}^2\frac{T_M^{n+1}-T_{M-1}^{n+1}}{2h^2} - k\frac{a^*}{b^*r_M^2}r_{M-\frac{1}{2}}^2\frac{T_M^{n}-T_{M-1}^{n}}{2h^2} + s_M^{n+\frac{1}{2}}. \tag{42c}$$

Again, it can be seen that the truncation error of the new scheme has an order of $\Delta t^2 + h^2$ at all grid points $(r_j, t_{n+(1/2)}), j = 1,\cdots,M$.

It should be pointed out that, in general, there is no boundary condition at the center $r = 0$. Therefore, the value of T_0^n at center needs to be determined. To this end, one may follow the idea in [14], multiply Eq. (30a) by r^2 and then integrate it over the interval $[0, \varepsilon]$, where ε is a small constant. This gives

$$\int_0^\varepsilon C\frac{\partial T(r,t)}{\partial t}r^2dr = k\int_0^\varepsilon\frac{\partial}{\partial r}\left(r^2\frac{\partial T(r,t)}{\partial r}\right)dr + \int_0^\varepsilon s(r,t)r^2dr. \tag{43}$$

Replacing $\partial T(r,t)/\partial t$ and $s(r,t)$ in Eq. (43) with those corresponding values at the center $r = 0$, and then calculating the integrals in Eq. (43), we obtain

$$C\frac{\partial T(0,t)}{\partial t}\cdot\frac{\varepsilon^3}{3} = k\varepsilon^2\frac{\partial T(\varepsilon,t)}{\partial r} + s(0,t)\frac{\varepsilon^3}{3}. \tag{44}$$

By choosing $\varepsilon = h/2$, a second-order finite difference approximation at the center $r = 0$ can be obtained as

$$C\frac{T_0^{n+1}-T_0^n}{\Delta t} = 6k\frac{T_1^{n+1}-T_0^{n+1}}{2h} + 6k\frac{T_1^n-T_0^n}{2h} + s_0^{n+\frac{1}{2}}. \tag{45}$$

For this case, one may choose $\theta_1 = 1$ and hence the scheme consists of Eq. (42b) with $1 \le j \le M-1$, Eq. (42c) and Eq. (45).

CASE 4. The idea lying behind the above method can be applied to develop higher-order compact finite difference schemes where the Neumann boundary condition is considered. For example, in CASE 1, if the second-order derivative T_{xx} is approximated by a fourth-order implicit compact finite difference scheme [16,19]:

$$\frac{1}{10}T_{xx}(x_{j-1},t) + T_{xx}(x_j,t) + \frac{1}{10}T_{xx}(x_{j+1},t) = \frac{6}{5h^2}[T(x_{j-1},t) - 2T(x_j,t) + T(x_{j+1},t)], \tag{46}$$

at the interior points x_j, $1 \le j \le M-1$, then the values of T_{xx} at the boundary points should be provided, which are usually inconvenient to obtain. To overcome this difficulty, we may employ a combined compact finite difference approximation at x_1 based on the mesh shown in Fig. 1:

$$aT_{xx}(x_1,t) + bT_{xx}(x_2,t) = -\frac{1}{h}T_x(x_1-\theta_1 h,t) + \frac{c}{h^2}[T(x_2,t) - T(x_1,t)], \tag{47}$$

where a, b, c and θ_1 are constants to be determined, and $\theta_1 \ge 0$. We expand each term of Eq. (47) into Taylor series at x_1 and obtain the left-hand-side (LHS) and right-hand-side (RHS) results of Eq. (47) as follows:

$$\text{LHS} = aT_{xx}(x_1,t) + b\left[T_{xx}(x_1,t) + hT_{x^3}(x_1,t) + \frac{h^2}{2}T_{x^4}(x_1,t)\right] + O(h^3) = (a+b)T_{xx}(x_1,t) + bhT_{x^3}(x_1,t) + b\frac{h^2}{2}T_{x^4}(x_1,t) + O(h^3), \tag{48a}$$

and

$$\text{RHS} = -\frac{1}{h}\left[T_x(x_1,t) - \theta_1 hT_{xx}(x_1,t) + \frac{\theta_1^2h^2}{2}T_{x^3}(x_1,t) - \frac{\theta_1^3h^3}{6}T_{x^4}(x_1,t)\right] + \frac{c}{h^2}\left[hT_x(x_1,t) + \frac{h^2}{2}T_{xx}(x_1,t) + \frac{h^3}{6}T_{x^3}(x_1,t) + \frac{h^4}{24}T_{x^4}(x_1,t)\right] + O(h^3) = (c-1)\frac{1}{h}T_x(x_1,t) + \left(\theta_1+\frac{c}{2}\right)T_{xx}(x_1,t) + \left(-\frac{\theta_1^2}{2}+\frac{c}{6}\right)hT_{x^3}(x_1,t) + \left(\frac{\theta_1^3}{3}+\frac{c}{12}\right)\frac{h^2}{2}T_{x^4}(x_1,t) + O(h^3). \tag{48b}$$

Matching both sides gives

$$c-1=0, \tag{49a}$$

$$a+b=\theta_1+\frac{c}{2}, \tag{49b}$$

$$b=-\frac{\theta_1^2}{2}+\frac{c}{6}, \tag{49c}$$

$$b=\frac{\theta_1^3}{3}+\frac{c}{12}. \tag{49d}$$

From Eqs. (49a), (49c) and (49d), we obtain a polynomial of degree 3 with respect to θ_1 as

$$4\theta_1^3+6\theta_1^2-1=0. \tag{50}$$

Solving the above equation for θ_1 with $\theta_1\geq 0$, one may obtain $\theta_1=(\sqrt{3}-1)/2$ and hence

$$a=\frac{\sqrt{3}}{4}+\frac{1}{3},\quad b=\frac{\sqrt{3}}{4}-\frac{1}{3},\quad c=1. \tag{51}$$

Thus, a third-order combined compact finite difference scheme at x_1 can be obtained by dropping the truncation error $O(h^3)$ as

$$aT_{xx}(x_1,t)+bT_{xx}(x_2,t)\approx -\frac{1}{h}T_x(x_1-\theta_1 h,t)+\frac{c}{h^2}[T(x_2,t)-T(x_1,t)]. \tag{52}$$

Similarly, we employ a combined compact finite difference approximation at x_M, which is the point next to the right boundary, as

$$b^*T_{xx}(x_{M-1},t)+a^*T_{xx}(x_M,t)=\frac{1}{h}T_x(x_M+\theta_2 h,t)-\frac{c^*}{h^2}[T(x_M,t)-T(x_{M-1},t)], \tag{53}$$

where a^*, b^*, c^* and θ_2 are constants to be determined, and obtain a third-order compact finite difference scheme at x_M

$$b^*T_{xx}(x_{M-1},t)+a^*T_{xx}(x_M,t)\approx\frac{1}{h}T_x(x_M+\theta_2 h,t)-\frac{c^*}{h^2}[T(x_M,t)-T(x_{M-1},t)], \tag{54}$$

where

$$\theta_2=\frac{\sqrt{3}-1}{2},\quad a^*=\frac{\sqrt{3}}{4}+\frac{1}{3},\quad b^*=\frac{\sqrt{3}}{4}-\frac{1}{3},\quad c^*=1. \tag{55}$$

If the number of interior grid points M is given, then the grid size and the coordinates of the grid points can be determined as follows:

$$h=\frac{L}{M+\theta_1+\theta_2-1},\quad x_j=(j-1+\theta_1)h,\quad j=1,\cdots,M. \tag{56}$$

Hence, a higher-order accurate Crank–Nicholson type of compact finite difference scheme for the heat conduction problem given in CASE 1 can be written as

$$aC\frac{T_1^{n+1}-T_1^n}{\Delta t}+bC\frac{T_2^{n+1}-T_2^n}{\Delta t}=k\frac{c}{h^2}\frac{T_2^{n+1}-T_1^{n+1}}{2}+k\frac{c}{h^2}\frac{T_2^n-T_1^n}{2}+s_1^{n+\frac{1}{2}}, \tag{57a}$$

$$C\frac{T_{j-1}^{n+1}-T_{j-1}^n}{10\Delta t}+C\frac{T_j^{n+1}-T_j^n}{\Delta t}+C\frac{T_{j+1}^{n+1}-T_{j+1}^n}{10\Delta t}=k\frac{6}{5h^2}\frac{T_{j-1}^{n+1}-2T_j^{n+1}+T_{j+1}^{n+1}}{2}+k\frac{6}{5h^2}\frac{T_{j-1}^n-2T_j^n+T_{j+1}^n}{2}+s_j^{n+\frac{1}{2}},\quad 2\leq j\leq M-1, \tag{57b}$$

$$b^*C\frac{T_{M-1}^{n+1}-T_{M-1}^n}{\Delta t}+a^*C\frac{T_M^{n+1}-T_M^n}{\Delta t}=-k\frac{c^*}{h^2}\frac{T_M^{n+1}-T_{M-1}^{n+1}}{2}-k\frac{c^*}{h^2}\frac{T_M^n-T_{M-1}^n}{2}+s_M^{n+\frac{1}{2}}. \tag{57c}$$

It can be seen that the truncation error of the new scheme has an order of Δt^2+h^4 at interior grid points $(x_j,t_{n+(1/2)})$, $j=2,\cdots,M-1$ [16,19], and an order of Δt^2+h^3 at grid points x_1 and x_M. Similarly, one may apply this method to the cylindrical and spherical coordinate cases and develop higher-order combined compact finite difference schemes for Neumann boundary conditions.

3. Stability

We now show that the above obtained schemes are unconditionally stable. Because of the limit on text length, we only show that the scheme developed in CASE 3 is unconditionally stable. One may use a similar argument to obtain that the new numerical schemes in CASES 1 and 2 are unconditionally stable. For simplicity, we first introduce two finite difference operators:

$$\nabla_{\bar{r}}T_j^q=\frac{1}{h}\left[T_j^q-T_{j-1}^q\right],$$
$$P_r\left[T_j^q\right]=r_{j+\frac{1}{2}}^2\frac{T_{j+1}^q-T_j^q}{h^2}-r_{j-\frac{1}{2}}^2\frac{T_j^n-T_{j-1}^q}{h^2},\quad q=n,n+1. \tag{58}$$

We then multiply Eq. (42a) by $2r_1^2h\frac{b}{a}[T_1^{n+1}+T_1^n]$, Eq. (42b) by $2r_j^2h[T_j^{n+1}+T_j^n]$, $2\leq j\leq M-1$ Eq. (42c) by $2r_M^2h\frac{b^*}{a^*}[T_M^{n+1}+T_M^n]$, and add all of them together. This gives

$$\begin{aligned}&\frac{2h}{\Delta t}C\frac{b}{a}r_1^2\left(\left[T_1^{n+1}\right]^2-\left[T_1^n\right]^2\right)+\frac{2h}{\Delta t}C\sum_{j=2}^{M-1}r_j^2\left(\left[T_j^{n+1}\right]^2-\left[T_j^n\right]^2\right)\\&+\frac{2h}{\Delta t}C\frac{b^*}{a^*}r_M^2\left(\left[T_M^{n+1}\right]^2-\left[T_M^n\right]^2\right)\\&=h\sum_{j=2}^{M-1}P_r\left[T_j^{n+1}+T_j^n\right]\left[T_j^{n+1}+T_j^n\right]+r_{\frac{3}{2}}^2\nabla_{\bar{r}}\left[T_2^{n+1}+T_2^n\right]\\&\left[T_1^{n+1}+T_1^n\right]-r_{M-\frac{1}{2}}^2\nabla_{\bar{r}}\left[T_M^{n+1}+T_M^n\right]\left[T_M^{n+1}+T_M^n\right]\\&+h\left\{2\frac{b}{a}r_1^2s_1^{n+\frac{1}{2}}\left[T_1^{n+1}+T_1^n\right]+\sum_{j=2}^{M-1}2r_j^2s_j^{n+\frac{1}{2}}\left[T_j^{n+1}+T_j^n\right]\right.\\&\left.+2\frac{b^*}{a^*}r_M^2s_M^{n+\frac{1}{2}}\left[T_M^{n+1}+T_M^n\right]\right\}.\end{aligned} \tag{59}$$

Denoting $U_j=T_j^{n+1}+T_j^n$ for the purpose of simple notation, the first three terms (FTT) on the right-hand-side can be simplified to

$$\begin{aligned}\mathrm{FTT}&=\frac{1}{h}\sum_{j=2}^{M-1}\left\{r_{j+\frac{1}{2}}^2[U_{j+1}-U_j]-r_{j-\frac{1}{2}}^2[U_j-U_{j-1}]\right\}U_j+r_{\frac{3}{2}}^2\nabla_{\bar{r}}U_2\cdot U_1\\&\quad-r_{M-\frac{1}{2}}^2\nabla_{\bar{r}}U_M\cdot U_M\\&=\sum_{j=3}^{M}r_{j-\frac{1}{2}}^2\nabla_{\bar{r}}U_j\cdot U_{j-1}-\sum_{j=2}^{M-1}r_{j-\frac{1}{2}}^2\nabla_{\bar{r}}U_j\cdot U_j+r_{\frac{3}{2}}^2\nabla_{\bar{r}}U_2\cdot U_1\\&\quad-r_{M-\frac{1}{2}}^2\nabla_{\bar{r}}U_M\cdot U_M=\sum_{j=2}^{M}r_{j-\frac{1}{2}}^2\nabla_{\bar{r}}U_j\cdot U_{j-1}-\sum_{j=2}^{M}r_{j-\frac{1}{2}}^2\nabla_{\bar{r}}U_j\cdot U_j\\&=-h\sum_{j=2}^{M}r_{j-\frac{1}{2}}^2\nabla_{\bar{r}}U_j\cdot\nabla_{\bar{r}}U_j=-h\sum_{j=2}^{M}r_{j-\frac{1}{2}}^2\left(\nabla_{\bar{r}}\left[T_j^{n+1}+T_j^n\right]\right)^2\end{aligned} \tag{60}$$

By Cauchy-Schwartz's inequality ($2ab \le \varepsilon a^2 + \frac{1}{\varepsilon}b^2, \varepsilon > 0$ [20]), we have

$$2s_j^{n+\frac{1}{2}}\left[T_j^{n+1}+T_j^n\right] \le C\left[T_j^{n+1}+T_j^n\right]^2+\frac{1}{C}\left[s_j^{n+\frac{1}{2}}\right]^2 \le 2C\left(\left[T_j^{n+1}\right]^2+\left[T_j^n\right]^2\right)+\frac{1}{C}\left[s_j^{n+\frac{1}{2}}\right]^2, \quad (61)$$

for any j. Substituting Eqs. (60) and (61) into Eq. (59) and dropping the negative term $-h\sum_{j=2}^{M} r_{j-(1/2)}^2(\nabla_{\bar{r}}[T_j^{n+1}+T_j^n])^2$ on the RHS, we can simplify Eq. (59) to

$$\begin{aligned}&\frac{2h}{\Delta t}C\frac{b}{a}r_1^2\left(\left[T_1^{n+1}\right]^2-\left[T_1^n\right]^2\right)+\frac{2h}{\Delta t}C\sum_{j=2}^{M-1}r_j^2\left(\left[T_j^{n+1}\right]^2-\left[T_j^n\right]^2\right)\\&+\frac{2h}{\Delta t}C\frac{b^*}{a^*}r_M^2\left(\left[T_M^{n+1}\right]^2-\left[T_M^n\right]^2\right)\le 2hC\frac{b}{a}r_1^2\left(\left[T_1^{n+1}\right]^2+\left[T_1^n\right]^2\right)\\&+2hC\sum_{j=2}^{M-1}r_j^2\left(\left[T_j^{n+1}\right]^2+\left[T_j^n\right]^2\right)+2hC\frac{b^*}{a^*}r_M^2\left(\left[T_M^{n+1}\right]^2+\left[T_M^n\right]^2\right)\\&+h\frac{1}{C}\left(\frac{b}{a}r_1^2\left[s_1^{n+\frac{1}{2}}\right]^2+\sum_{j=2}^{M-1}r_j^2\left[s_j^{n+\frac{1}{2}}\right]^2+\frac{b^*}{a^*}r_M^2\left[s_M^{n+\frac{1}{2}}\right]^2\right).\end{aligned} \quad (62)$$

Multiplying Eq. (62) by Δt and letting

$$F(n)\equiv 2hC\left(\frac{b}{a}r_1^2\left[T_1^n\right]^2+\sum_{j=2}^{M-1}r_j^2\left[T_j^n\right]^2+\frac{b^*}{a^*}r_M^2\left[T_M^n\right]^2\right), \quad (63a)$$

$$\Phi(n)\equiv h\frac{1}{C}\left(\frac{b}{a}r_1^2\left[s_1^{n+\frac{1}{2}}\right]^2+\sum_{j=2}^{M-1}r_j^2\left[s_j^{n+\frac{1}{2}}\right]^2+\frac{b^*}{a^*}r_M^2\left[s_M^{n+\frac{1}{2}}\right]^2\right), \quad (63b)$$

Eq. (62) can be further simplified to

$$\begin{aligned}F(n+1)&\le\frac{1+\Delta t}{1-\Delta t}F(n)+\frac{\Delta t}{1-\Delta t}\Phi(n)\\&\le\frac{1+\Delta t}{1-\Delta t}\left[\frac{1+\Delta t}{1-\Delta t}F(n-1)+\frac{\Delta t}{1-\Delta t}\Phi(n-1)\right]+\frac{\Delta t}{1-\Delta t}\Phi(n)\\&\le\cdots\le\left(\frac{1+\Delta t}{1-\Delta t}\right)^{n+1}F(0)+\frac{\Delta t}{1-\Delta t}\left[1+\frac{1+\Delta t}{1-\Delta t}+\left(\frac{1+\Delta t}{1-\Delta t}\right)^2\right.\\&\left.+\cdots+\left(\frac{1+\Delta t}{1-\Delta t}\right)^n\right]\max_{0\le k\le n}\Phi(k)\\&\le\left(\frac{1+\Delta t}{1-\Delta t}\right)^{n+1}\left[F(0)+\max_{0\le k\le n}\Phi(k)\right].\end{aligned} \quad (64)$$

Using the inequalities $(1+\varepsilon)^n \le e^{n\varepsilon}$ for $\varepsilon > 0$ and $(1-\varepsilon)^{-1} \le e^{2\varepsilon}$ for $0 < \varepsilon \le 1/2$, we obtain $(1+\Delta t)^{n+1} \le e^{(n+1)\Delta t}$ and $(1-\Delta t)^{-1} \le e^{2\Delta t}$, and hence, when Δt is sufficiently small, the solution to the present scheme satisfies

$$\begin{aligned}F(n+1)&\le e^{3(n+1)\Delta t}\left[F(0)+\max_{0\le k\le n}\Phi(k)\right]\\&\le e^{3t_0}\left[F(0)+\max_{0\le k\le n}\Phi(k)\right],\end{aligned} \quad (65)$$

for any $0 \le (n+1)\Delta t \le t_0$. Hence, for any $0 \le n\Delta t \le t_0$, we obtain

$$\begin{aligned}&2C\left(\frac{b}{a}r_1^2\left[T_1^n\right]^2+\sum_{j=2}^{M-1}r_j^2\left[T_j^n\right]^2+\frac{b^*}{a^*}r_M^2\left[T_M^n\right]^2\right)\\&\le e^{3t_0}2C\left(\frac{b}{a}r_1^2\left[T_1^0\right]^2+\sum_{j=2}^{M-1}r_j^2\left[T_j^0\right]^2+\frac{b^*}{a^*}r_M^2\left[T_M^0\right]^2\right)\\&+e^{3t_0}\max_{0\le k\le n-1}\frac{1}{C}\left(\frac{b}{a}r_1^2\left[s_1^{k+\frac{1}{2}}\right]^2+\sum_{j=2}^{M-1}r_j^2\left[s_j^{k+\frac{1}{2}}\right]^2+\frac{b^*}{a^*}r_M^2\left[s_M^{k+\frac{1}{2}}\right]^2\right),\end{aligned} \quad (66)$$

implying that the scheme is unconditionally stable with respect to the initial condition and source term.

For the stability analysis of the higher-order accurate compact finite difference scheme, Eq. (57), one may use a very similar matrix analysis as described in [16] and obtain that the scheme is unconditionally stable. We omit the proof here because it is quite straightforward.

4. Numerical examples

To verify the accuracy of our numerical schemes, we first consider a simple scenario as follows:

$$\frac{\partial T(x,t)}{\partial t}=\frac{\partial^2 T(x,t)}{\partial x^2},\quad 0<x<1, t>0, \quad (67a)$$

$$T(x,0)=\cos(\pi x),\quad x\in[0,1], \quad (67b)$$

$$\frac{\partial T(0,t)}{\partial x}=\frac{\partial T(1,t)}{\partial x}=0,\quad t\ge 0, \quad (67c)$$

where the analytical solution is $T(x,t) = e^{-\pi^2 t}\cos(\pi x)$. We employed the Crank–Nicholson scheme, Eq. (2), with the first-order finite difference scheme for the Neumann boundary condition, Eq. (3); the Crank–Nicholson scheme, Eq. (2), with the new second-order finite difference scheme for the Neumann boundary condition, Eq. (14); and the higher-order compact scheme, Eq. (57), to solve the above problem, respectively. Since these three schemes are implicit, the Thomas algorithm [14] was used for solving the obtained tridiagonal linear systems.

Because the analytical solution $T(x, t)$ becomes very small when t is large, the maximum of l_2-norm errors of the numerical solutions as compared with the analytical solution was computed for $0 \le t \le 1$ based on the formula

$$E(M,\Delta t)=\max_{0\le n\Delta t\le 1.0}\sqrt{h\sum_{j=1}^{M}\left[T_j^n-T^{\text{exact}}(x_j,t_n)\right]^2}. \quad (68)$$

To obtain the convergence rate with respect to the spatial variable, we may assume that $E(M, \Delta t) = O(\Delta t^p + h^q)$. If Δt is small enough, then $E(M, \Delta t) \approx O(h^q)$. Consequently, $E(M,\Delta t)/E(2M,\Delta t) \approx 2^q$ and hence $q \approx \log_2[E(M,\Delta t)/E(2M,\Delta t)]$ is the convergence rate with respect to the spatial variable. Likewise, $p \approx \log_2[E(M,2\Delta t)/E(M,\Delta t)]$ is the convergence rate with respect to the temporal variable.

In our computation, we first chose the number of grid points to be $M = 51$, 101, and 201 for the Crank–Nicholson scheme with Eq. (3), and the number of interior grid points to be $M = 51$, 101, and 201 for the Crank–Nicholson scheme with Eq. (14). On the other hand, we chose a smaller number of interior grid points to be $M = 11$, 21, and 41 for the higher-order compact scheme since it is higher-order scheme. For all three cases, the time increment was set to be $\Delta t = 10^{-6}$ and $\log_2[E(M,\Delta t)/E(2M,\Delta t)]$ was calculated for the convergence rate with respect to the spatial variable.

Table 1 shows the maximal l_2-norm errors of the numerical results and convergence rates when $0 \le n\Delta t \le 1.0$. It can be seen from the table that the convergence rate of the Crank–Nicholson scheme with Eq. (3) is about 1.0 and the one for the Crank–Nicholson scheme with Eq. (14) is about 2.0, while the higher-order compact scheme gives the highest convergence rate. By comparing the maximal l_2-norm errors of solutions in Table 1 among these three schemes, we can see that the Crank–Nicholson scheme with Eq. (14) provides much more accurate solutions than the Crank–Nicholson scheme with Eq. (3) and the higher-order compact scheme gives excellent solutions by using a smaller number of grid points.

Table 1
Maximal l_2-norm errors, $E(M, \Delta t)$, and convergence rates when $\Delta t = 10^{-6}$ and $0 \le t \le 1.0$ for the first scenario.

(a)

Grids	CN with Eq. (3) $E(M, \Delta t)$	CN with Eq. (3) rate	CN with Eq. (14) $E(M, \Delta t)$	CN with Eq. (14) rate
51	1.03041×10^{-2}	–	8.03048×10^{-5}	–
101	5.20193×10^{-3}	0.986	2.07331×10^{-5}	1.954
201	2.61315×10^{-5}	0.993	5.27770×10^{-6}	1.974

(b)

Grids	Compact scheme Eq. (57) $E(M, \Delta t)$	Compact scheme Eq. (57) rate
11	9.96415×10^{-6}	–
21	6.59230×10^{-7}	3.918
41	5.84852×10^{-8}	3.494

To obtain the convergence rate p, we chose the number of grid points to be $M = 1,000,001$ for the Crank–Nicholson scheme with Eq. (3) or Eq. (14), and $M = 1,001$ for the higher-order compact scheme. On the other hand, the time increment was set to be $\Delta t = 0.01, 0.005, 0.0025$, respectively, and $\log_2[E(M, 2\Delta t)/E(M, \Delta t)]$ was calculated. For this case, we expect that p is about 2 for all three schemes because they take the average of the numerical solutions in two time-levels and hence are second-order accurate with respect to the temporal variable. Table 2 shows the maximal l_2-norm errors of the numerical solutions and convergence rates when $0 \le n\Delta t \le 1.0$. As is expected, we see from the table that the convergence rates obtained from all three schemes are about the same and are about 2.0. Furthermore, it can be seen from Table 2 that although the maximal l_2-norm errors obtained from all three schemes are about the same, the number of grid points for the Crank–Nicholson scheme is about square of the number of the grid points for the compact scheme.

The second scenario is considered to be a dimensionless heat conduction in cylindrical coordinates:

$$\frac{\partial T(r,t)}{\partial t} = \frac{1}{r}\frac{\partial}{\partial r}\left(r\frac{\partial T(r,t)}{\partial r}\right) + \frac{\pi}{r}e^{-\pi^2 t}\sin(\pi r), \quad 0 < r < 1, t > 0, \tag{69a}$$

$$T(r,0) = \cos(\pi r), \quad r \in [0,1], \tag{69b}$$

$$\frac{\partial T(0,t)}{\partial r} = \frac{\partial T(1,t)}{\partial r} = 0, \quad t \ge 0, \tag{69c}$$

where the analytical solution is $T(r,t) = e^{-\pi^2 t}\cos(\pi r)$. For this case, the new scheme, Eqs. (29a)–(29c), and the Crank–Nicholson scheme, Eq. (29b), with Eq. (3) were employed to solve the above problem, respectively. We chose the number of grid points to be

Table 2
Maximal l_2-norm errors, $E(M, \Delta t)$, and convergence rates when (a) $M = 1,000,001$ for both CN schemes, (b) $M = 1,001$ for the compact scheme, and $0 \le t \le 1.0$ for the first scenario.

(a)

Δt	CN with Eq. (3) $E(M, \Delta t)$	CN with Eq. (3) rate	CN with Eq. (14) $E(M, \Delta t)$	CN with Eq. (14) rate
0.01	2.10939×10^{-4}	–	2.10422×10^{-4}	–
0.005	5.23540×10^{-5}	2.011	5.18323×10^{-5}	2.021
0.0025	1.27009×10^{-5}	2.043	1.21767×10^{-5}	2.090

(b)

Δt	Compact scheme Eq. (57) $E(M, \Delta t)$	Compact scheme Eq. (57) rate
0.01	2.11407×10^{-4}	–
0.005	5.27988×10^{-5}	2.001
0.0025	1.31865×10^{-5}	2.001

Table 3
Maximal l_2-norm errors, $E(M, \Delta t)$, and convergence rates when (a) $\Delta t = 10^{-6}$, (b) $M = 1,000,001$, and $0 \le t \le 1.0$ for the second scenario.

(a)

Grid	CN with Eq. (3) $E(M, \Delta t)$	CN with Eq. (3) rate	Scheme Eq. (29) $E(M, \Delta t)$	Scheme Eq. (29) rate
51	1.99313×10^{-2}	–	1.91822×10^{-4}	–
101	9.98212×10^{-3}	0.998	5.00483×10^{-5}	1.938
201	4.99518×10^{-3}	0.999	1.27701×10^{-5}	1.971

(b)

Δt	CN with Eq. (3) $E(M, \Delta t)$	CN with Eq. (3) rate	Scheme Eq. (29) $E(M, \Delta t)$	Scheme Eq. (29) rate
0.01	3.95927×10^{-4}	–	3.95949×10^{-4}	–
0.005	9.89155×10^{-5}	2.001	9.89524×10^{-5}	2.001
0.0025	2.47098×10^{-5}	2.001	2.47348×10^{-5}	2.000

$M = 51, 101$, and 201 for the Crank–Nicholson scheme with Eq. (3), and the number of interior grid points to be $M = 51, 101$, and 201 for the new scheme. Again, the time increment was set to be $\Delta t = 10^{-6}$.

Table 3(a) shows the maximal l_2-norm errors of the numerical results and convergence rates when $0 \le n\Delta t \le 1.0$. It can be seen from the table that the convergence rate of the Crank–Nicholson scheme with Eq. (3) is about 1.0, while the one for the new scheme is about 2.0. Furthermore, by comparing the maximal l_2-norm errors of solutions between these two schemes in Table 3(a), we see that the new scheme provides much more accurate solutions than the Crank–Nicholson scheme with Eq. (3).

Again, we chose the number of grid points to be $M = 1,000,001$ for both schemes and set the time increment to be $\Delta t = 0.01, 0.005, 0.0025$, respectively, to obtain the convergence rate p. Results indicate that the convergence rates obtained from both schemes are about the same and are about 2.0, as shown in Table 3(b).

The third scenario is considered to be a dimensionless heat conduction in spherical coordinates:

$$\frac{\partial T(r,t)}{\partial t} = \frac{1}{r^2}\frac{\partial}{\partial r}\left(r^2\frac{\partial T(r,t)}{\partial r}\right) + \frac{2\pi}{r}e^{-\pi^2 t}\sin(\pi r), \quad 0 < r < 1, t > 0, \tag{70a}$$

$$T(r,0) = \cos(\pi r), \quad r \in [0,1], \tag{70b}$$

$$\frac{\partial T(0,t)}{\partial r} = \frac{\partial T(1,t)}{\partial r} = 0, \quad t \ge 0, \tag{70c}$$

where the analytical solution is $T(r,t) = e^{-\pi^2 t}\cos(\pi r)$. For this case, the new scheme, Eqs. (42a)–(42c), and the Crank–Nicholson scheme, Eq. (42b), with Eq. (3) were employed to solve the above problem, respectively. We chose the same conditions as those in the second scenario and the result is shown in Table 4. It can be seen from Table

Table 4
Maximal l_2-norm errors, $E(M, \Delta t)$, and convergence rates when (a) $\Delta t = 10^{-6}$, (b) $M = 1,000,001$, and $0 \le t \le 1.0$ for the third scenario.

(a)

Grid	CN with Eq. (3) $E(M, \Delta t)$	CN with Eq. (3) rate	Scheme Eq. (42) $E(M, \Delta t)$	Scheme Eq. (42) rate
51	3.01995×10^{-2}	–	2.01446×10^{-4}	–
101	1.50487×10^{-2}	1.005	6.80595×10^{-5}	1.566
201	7.51171×10^{-3}	1.002	2.22334×10^{-5}	1.614

(b)

Δt	CN with Eq. (3) $E(M, \Delta t)$	CN with Eq. (3) rate	Scheme Eq. (42) $E(M, \Delta t)$	Scheme Eq. (42) rate
0.01	5.68601×10^{-4}	–	5.68765×10^{-4}	–
0.005	1.41817×10^{-4}	2.003	1.41988×10^{-4}	2.002
0.0025	3.53267×10^{-5}	2.005	3.55045×10^{-5}	2.000

4(a) that the convergence rate of the Crank–Nicholson scheme with Eq. (3) is about 1.0, while the one for the new scheme is about 1.6. Again, by comparing the maximal l_2-norm errors of solutions between these two schemes in Table 4(a), we see that the new scheme provides much more accurate solutions than the Crank–Nicholson scheme with Eq. (3). Table 4(b) shows that the convergence rates obtained from both schemes are about the same and are about 2.0.

5. Conclusion

In this study, we have presented a kind of new and accurate finite difference schemes for the Neumann (insulated) boundary condition in Cartesian, cylindrical, and spherical coordinates, respectively. Coupled with the Crank–Nicholson finite difference method or the higher-order compact finite difference method, the new scheme is proved to be unconditionally stable and provides much more accurate numerical solutions. The numerical errors and convergence rates of the solutions are tested by several examples. Results show that the maximal l_2-norm errors of the numerical solutions obtained by the present method are much smaller than those obtained by the conventional method, and, also, the convergence rates of the present method are higher with respect to the spatial variable. The method can be readily applied to multi-dimensional cases. Further research will be focused on the applications of the new method to practical engineering problems, such as ultrafast heat transfer and reaction-diffusions.

References

[1] T.Q. Qiu, C.L. Tien, Short-pulse laser heating on metals. Int. J. Heat Mass Transf. 35 (1992) 719–726.
[2] T.Q. Qiu, C.L. Tien, Heat transfer mechanisms during short-pulse laser heating of metals. ASME J. Heat Mass Transf. 115 (1993) 835–841.
[3] D.Y. Tzou, A unified field approach for heat conduction from micro to macroscales. ASME J. Heat Mass Transf. 117 (1995) 8–16.
[4] D.Y. Tzou, Macro- to Microscale Heat Transfer: the Lagging Behavior. Taylor & Francis, Washington DC, 1997.
[5] D.Y. Tzou, W. Dai, Thermal lagging in multi-carrier systems. Int. J. Heat Mass Transf. 52 (2009) 1206–1213.
[6] W. Dai, F. Zhu, D.Y. Tzou, A stable finite difference scheme for thermal analysis in an N-carrier system. Int. J. Therm. Sci. 48 (2009) 1530–1541.
[7] A. Faghri, Y. Zhang, Transport Phenomena in Multiphase Systems. Elsevier, UK, 2006.
[8] T.L. Rosenberry, Quantitative simulation of endplate currents at neuromuscular junctions based on the reaction of acetylcholine with receptor and acetylcholinesterase. Biophys. J. 26 (1979) 263–290.
[9] F. Dexter, Mathematical model of acetylcholine kinetics in neuroeffector junctions. Model. Physiol. 266 (1994) H298.
[10] A.W. Abu-Qare, M.B.S. Abou-Donia, Heat effects, metabolism, and methods of analysis. Food Chem. Toxicol. 40 (2002) 1327–1333.
[11] A. Venturino, R.M. Bergoc, Kinetic models on acetylcholinesterase modulation by self-substrate and polyamines. Estimation of interaction parameters and rate constants for free and acetylated states of the enzyme. J. Biol. Syst. 10 (2002) 127–147.
[12] W.Y. Liao, J.P. Zhu, A.Q.M. Khaliq, A fourth-order compact algorithm for nonlinear reaction-diffusions with Neumann boundary conditions. Numer. Methods Part. Differ. Equat. 22 (2006) 600–616.
[13] L. Lapidus, G.F. Pinder, Numerical Solution of Partial Differential Equations in Science and Engineering. Wiley, New York, 1982.
[14] K.W. Morton, D.F. Mayers, Numerical Solution of Partial Differential Equations. Cambridge University Press, London, 1994.
[15] J.W. Thomas, Numerical Partial Differential Equations: Finite Difference Methods. Springer-Verlag, New York, 1995.
[16] J. Zhao, W. Dai, T. Niu, Fourth-order compact schemes of a heat conduction problem with Neumann boundary conditions. Numer. Methods Part. Differ. Equat. 23 (2007) 949–959.
[17] J. Zhao, W. Dai, S. Zhang, 4th-order compact schemes for solving multi-dimensional heat conduction problems with Neumann boundary conditions. Numer. Methods Part. Differ. Equat. 24 (2008) 165–178.
[18] P. Chu, C. Fan, A three-point combined compact difference scheme. J. Comput. Phys. 140 (1998) 370–399.
[19] S.K. Lele, Compact finite difference schemes with spectral-like resolution. J. Comput. Phys. 103 (1992) 16–42.
[20] L.C. Evans, Partial Differential Equations. American Mathematical Society, Providence, Rhode Island, 1998.